



Mechanical, biological and tribological behaviour of fixation plates 3D printed by electron beam and selective laser melting

Abdulsalam Abdulaziz Al-Tamimi¹ · Miguel A. Hernandez² · Abdalla Omar³ · David Felipe Morales-Aldana⁴ · Chris Peach^{3,5} · Paulo Bartolo³

Received: 30 October 2019 / Accepted: 22 June 2020 / Published online: 6 July 2020
© The Author(s) 2020

Abstract

Commercially available fixation plates are built using metallic biocompatible materials such as titanium and its alloys and stainless steel. However, these plates show a stiffness mismatch comparing to bone, leading to stress shielding and bone loss. In this paper, we investigate the combined use of topology optimisation and additive manufacturing to print fixation plates with reduced stiffness and improved biological performance. Ti-6Al-4 V plates were topology optimised considering different loading conditions and volume reductions and printed using electron beam melting and selective laser melting. The effect of processing conditions on the mechanical properties, microhardness, wear resistance and surface roughness was analysed. Results show acceptable wear resistance values for a medical device and a reduction of stress shielding by increasing volume reduction. It is also shown that no polishing is required as 3D printed plates are able to support cell attachment and proliferation. In comparison to commercial plates, 3D printed ones show significantly better biological performance. For the same design, SLM plates present higher mechanical properties, while EBM plates present better cell attachment and proliferation.

Keywords Additive manufacturing · Electron beam melting · Fixation plates · Selective laser melting · Stress shielding · Topology optimisation

✉ Paulo Bartolo
paulojorge.dasilvabartolo@manchester.ac.uk

Abdulsalam Abdulaziz Al-Tamimi
Abdulsalam.altamimi@postgrad.manchester.ac.uk

Miguel A. Hernandez
miguel.hernandez@postgrad.manchester.ac.uk

David Felipe Morales-Aldana
david.moralesaldana@manchester.ac.uk

Chris Peach
Chris@shouldersandbells.co.uk

¹ Industrial Engineering Department, College of Engineering, King Saud University, Riyadh, Saudi Arabia

² School of Materials, The University of Manchester, Manchester, UK

³ School of Mechanical, Aerospace and Civil Engineering, The University of Manchester, Manchester, UK

⁴ School of Electrical and Electronic Engineering, The University of Manchester, Manchester, UK

⁵ Manchester University NHS Foundation Trust, Manchester, UK

1 Introduction

Bone fracture due to accidents or diseases represents an important healthcare problem. Worldwide, due to age population problems, the number of hip fractures is expected to be 6.3 million in 2050 with an estimated cost of \$13.15 billion [1]. In 2016, in the UK, 11,000 patients required revision operations due to implant failure, and this number will significantly increase in the next decade [2].

In most cases, fixation devices are used to return the fractured bone to its original anatomy and stabilise it. These fixation devices are commercially available as either pins, rods, plates and screws. However, they were not properly designed, and consequently, stress shielding and bone loss problems are common. Stress shielding is an important problem, affecting bone remodelling due to the significant mismatch between the mechanical properties of metallic fixation plates and bone (the compressive elastic modulus of cortical bone varies between 15 and 25 GPa) [3, 4].

Previously we demonstrated that topology optimisation is a viable tool to redesign fixation plates, minimising equivalent stiffness and consequently the stress shielding effect [5].

Topology optimisation is considered the most common strategy to optimise the structure material distribution of a given design domain using the solid isotropic microstructure with penalisation (SIMP) approach [6]. This approach considers a continuous convergence of the design variable (material element density), to determine if an element is to be removed ($\rho = 0$) or kept ($\rho = 1$). In addition, the relative density is distributed along each element as a constant, contributing to the Young's modulus (E) distribution, according to the following equation:

$$E(x, y, z) = [\rho(x, y, z)]^p \cdot E^0 \quad (1)$$

where p is the penalisation factor and E^0 is the initial Young's modulus when $\rho = 1$.

The common topology optimisation mathematical problem aims to minimise the compliance (C) of a structure considering a volume constraint and is mathematically described as follows [6]:

$$\min_{\rho_e} \rho_e C(\rho_e) = \mathbf{f}^T \cdot \mathbf{u} \quad (2)$$

$$\text{Subject to } \begin{cases} \sum_{e=1}^N v_e(\rho_e) \leq V^*, & (2a) \\ \sum_{e=1}^N K_e(\rho_e^p) \mathbf{u} = \mathbf{f}, & (2b) \\ 0 < \rho_0 \leq \rho_e \leq 1, & (2c). \end{cases}$$

where f is the force vector, K_e is the element stiffness matrix, u is the displacement vector, V^* is the user-defined fraction volume, ρ_e is the element density, ρ_0 is the minimum density, and v_e is the volume of each element. As observed, topology optimisation seeks to find the optimal load path for a particular load and boundary conditions searching for a minimum compliance design. However, as previously reported, reducing the density of an element which reduces the stiffness of that particular element becomes the dominant effect, contributing to the reduction of the overall equivalent stiffness.

The two most common powder bed fusion techniques are electron beam melting (EBM) and selective laser melting (SLM) using different processing conditions [7, 8]. These conditions affect the surface and microstructure characteristics. Consequently, the mechanical, biological and tribological performances of the built part are also affected.

In a previous paper, authors used electron beam melting to 3D print topology-optimised fixation plates considering different geometries and volume reductions [9].

Fig. 1 Design domains of fixation plates considered for optimisation. **a** Four-screw hole and **b** eight-screw hole

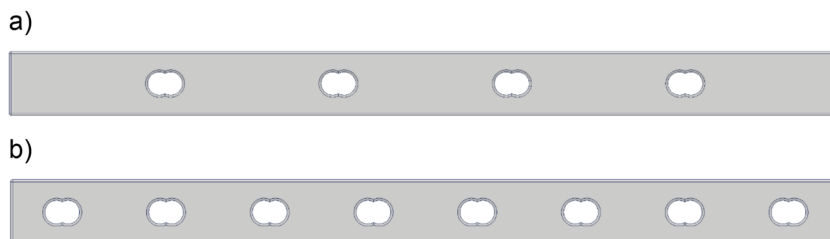


Table 1 Chemical composition of the initial Ti-6Al-4 V powders

Element	Chemical composition (%)							
	Ti	Al	V	C	Fe	O	N	H
EBM	89.607	6	4	0.03	0.1	0.15	0.01	0.003
SLM	89.866	5.9	3.9	0.01	0.19	0.12	0.01	0.004

Results show that some redesigned printed plates present mechanical properties similar to the cortical bone being able to withstand physiological loads and to establish a good biological bonding with the surrounding tissue without the need of any post-processing steps. This paper investigates two different powder bed fusion techniques, electron beam melting and selective laser melting, to 3D print topology-optimised plates. Key research questions being addressed are:

- How the different processing conditions, influencing the microstructure, surface microhardness and roughness affect the biological performance of the printed plates?
- What is the impact of the fabrication technique on a strategy to reduce the stress shielding?
- Are the plates 3D printed using standard powder bed fusion operating conditions and corresponding Ti-6Al-4 V powder suitable for medical applications without post-processing?

Printed fixation plates are compared to two commercially available plates, the DePuy Synthes 4.5/5.0 narrow locking compression plates (in commercial pure Titanium) and Zimmer Biomet anatomic locked plating system plates (in Ti-6Al-4 V).

2 Design of the fixation plates

Two different locking compression plates with four- and eight-screw holes were designed in Solidworks (Dassault Systems, France) as shown in Fig. 1. All plates have a length of 180 mm, a width of 14 mm and a thickness of 5 mm. Plates were redesigned using the solid isotropic microstructure with penalisation (SIMP) approach assuming different loading

Table 2 EDM parameters used for cutting the fixation plates

Parameter	Value
Energy duration of the pulse (μs)	0.50
Average voltage (V)	35.0
Wire speed (mm/min)	10.0
Time between 2 pulses (μs)	23.0
Wire tension (g)	1.30
Wire material	AC Brass 900

conditions (compression, bending, torsion and combination of all these loads) and volume reductions (45% and 75%) following the procedure previously described [5]. Topology-optimised designs were exported to the Magics software (Materialise, Belgium), where they were tessellated (STL file generation) and exported to the additive manufacturing machines.

3 Fixation plates fabrication

Two powder bed fusion techniques were used to 3D print the plates: electron beam melting (EBM) (Arcam A2 model, Arcam, Sweden) and selective laser melting (SLM) (250HL, SLM Solutions Lübeck, Germany). Ti-6Al-4 V powders were supplied by Arcam for the EBM system and TLS Technik GmbH (Bitterfeld, Germany) for the SLM system. Due to the large number of designs, a total of 32 plates (16 SLM and 16 EBM plates) were produced. For the same configuration (number of holes and volume reduction), SLM and EBM plates present the same dimensions.

The chemical composition of the initial powders is presented in Table 1. The powders are spherical in shape, having a size distribution between 45 and 100 μm (EBM powder) and between 25 to 45 μm (SLM powder).

The printing process, using a powder bed fusion technique, starts with the powder being spread in the working platform, scanned (based on the sliced pattern) and melted into a molten pool using a heat source (i.e. a laser beam controlled by two

rotating lenses above a certain angle lens for the SLM or an electron beam for the EBM). Once the scanning is completed, a new layer is deposited above the scanned layer, and the steps are repeated until the part is built.

The EBM system consists of an electron beam emitted via a hot tungsten filament, operated at 60 kV under vacuum pressure of 2.0×10^{-3} mBa, scanning speed of 4530 mm/s, beam focus offset of 3 mA, line offset of 0.3 mm and layer thickness of 50 μm . The substrate plate temperature was kept around 600 $^{\circ}\text{C}$, and the build temperature was defined to be around 750 $^{\circ}\text{C}$. The SLM system consists of a 400 W fibre laser, spot size of around 80 μm , laser power of 100 W, scanning speed of 375 mm/s, hatching distance of 130 μm and a layer thickness of 30 μm . The substrate plate was preheated to 200 $^{\circ}\text{C}$. In both cases, support structures were removed manually using pliers, and parts were not submitted to any further post-processing operation.

4 Fixation plate characterisation

4.1 Plates preparation

Fixation plates were cut using electron discharge machine (EDM) (FI 440 CC, GF machining solutions, Switzerland) using the parameters shown in Table 2. All plates were cleaned in an ultrasonic bath submerged in 80% ethanol and then washed thoroughly by distilled water. Plates for the biological study were autoclaved for 30 min at 121 $^{\circ}\text{C}$.

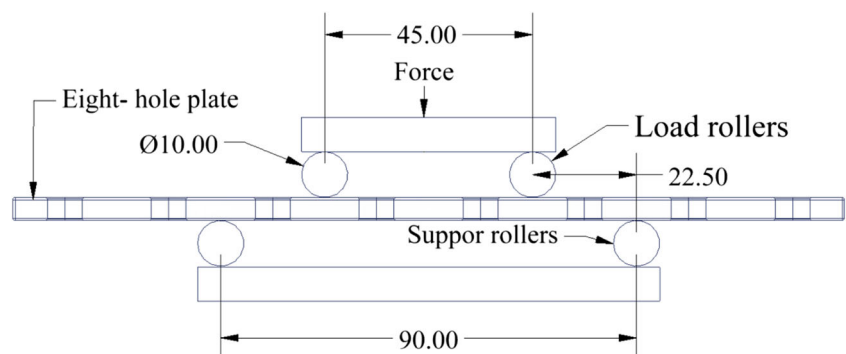
4.2 Density

The density was measured according to the standard Archimedes method (ASTM B962 – 17) immersing the fixation plates in water.

4.3 Surface roughness

Surface roughness was determined using a coaxial laser confocal microscope (VK-X200, Keyence, Japan) by scanning a zone of $500 \times 750 \mu\text{m}^2$. The average surface roughness, Ra,

Fig. 2 Eight-hole plate under a four-point bending test



was calculated considering 10 measurements over a length of 500 μm using the VK Analyzer 3.3 software (Keyence, Japan).

4.4 Microhardness and microstructure

In order to determine both the microhardness and microstructure, the surface of the fixation plates was prepared using silicon carbide paper with a grid of 400, 600, 800, 1200 and 2400 grits and polished with 9 and 1 μm diamond particle paste. At least five indentations were considered. Vickers microhardness (Indentec, UK) was measured considering a normal load of 0.3 Kgf applied for 10 s. The Vickers microhardness (HV) was measured by optical microscopy from all the indentations according to the following equation [10]:

$$HV = \frac{1.8544F}{d^2} \quad (3)$$

where F is the load and d is the arithmetic mean of the diagonals.

The grinded and polished plates were examined using the FE-SEM (Jeol, Japan) scanning electron microscopy (SEM), equipped with an energy-dispersive X-ray (EDX) with a voltage of 15.0 kV. Additionally, the plates were used to reveal the microstructure by etching in Kroll's reagent (300 mL H_2O , 100 mL HNO_3 and 100 mL HF). The phase analysis was performed using an X-ray diffraction (XRD) with Cu-K α radiation ($\lambda = 0.145 \text{ nm}$) and a scan speed of 2 deg/min using an X-ray diffractometer (Bruker, Germany).

4.5 Mechanical performance

Topology-optimised fixation plates were mechanically evaluated considering tensile, torsion and bending tests. Each optimised plate was tested considering the load case assumed for the topology optimisation, i.e. four-point bending for plates optimised for *bending* loading conditions; *torsion* for plates optimised for torsion loading conditions; tensile for plates optimised for *compression*; and four-point bending, torsion and tensile for *combined* loading conditions. All tests were performed at room temperature until plate failure. Failure was determined by either plate crack, breakage or permanent plastic deformation, whichever occurred first. Due to the large number of cases (topologies and loading conditions) considered in this study and the extensive experimental work, only one plate was considered. Consequently, it was not possible to perform statistical analysis.

4.5.1 Tensile test

Tensile tests were performed using the Instron® 8862 system (Instron, MA, USA) with a maximum force of 100 kN, with a controlled displacement rate of 0.5 mm/min and an accuracy of $\pm 0.002\%$ of load cell capacity or 0.5% of indicated load. Strains and displacements were measured using a standard straight profile knife edged extensometer (2630–106, Instron, USA). Tests were performed in duplicate. Force and displacement histories were documented at a sampling rate of

Fig. 3 3D printed fixation plates using **a** EBM and **b** SLM

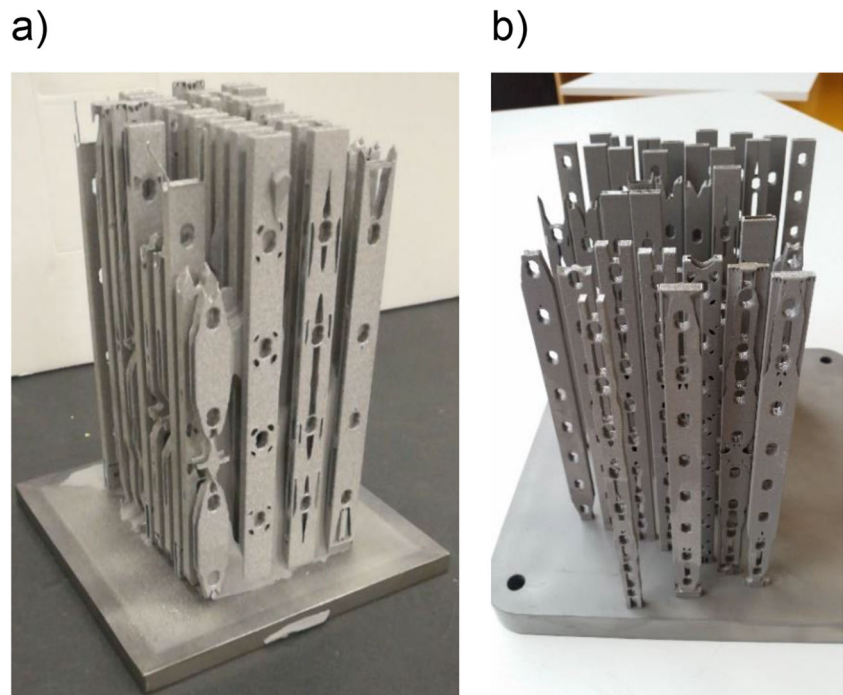
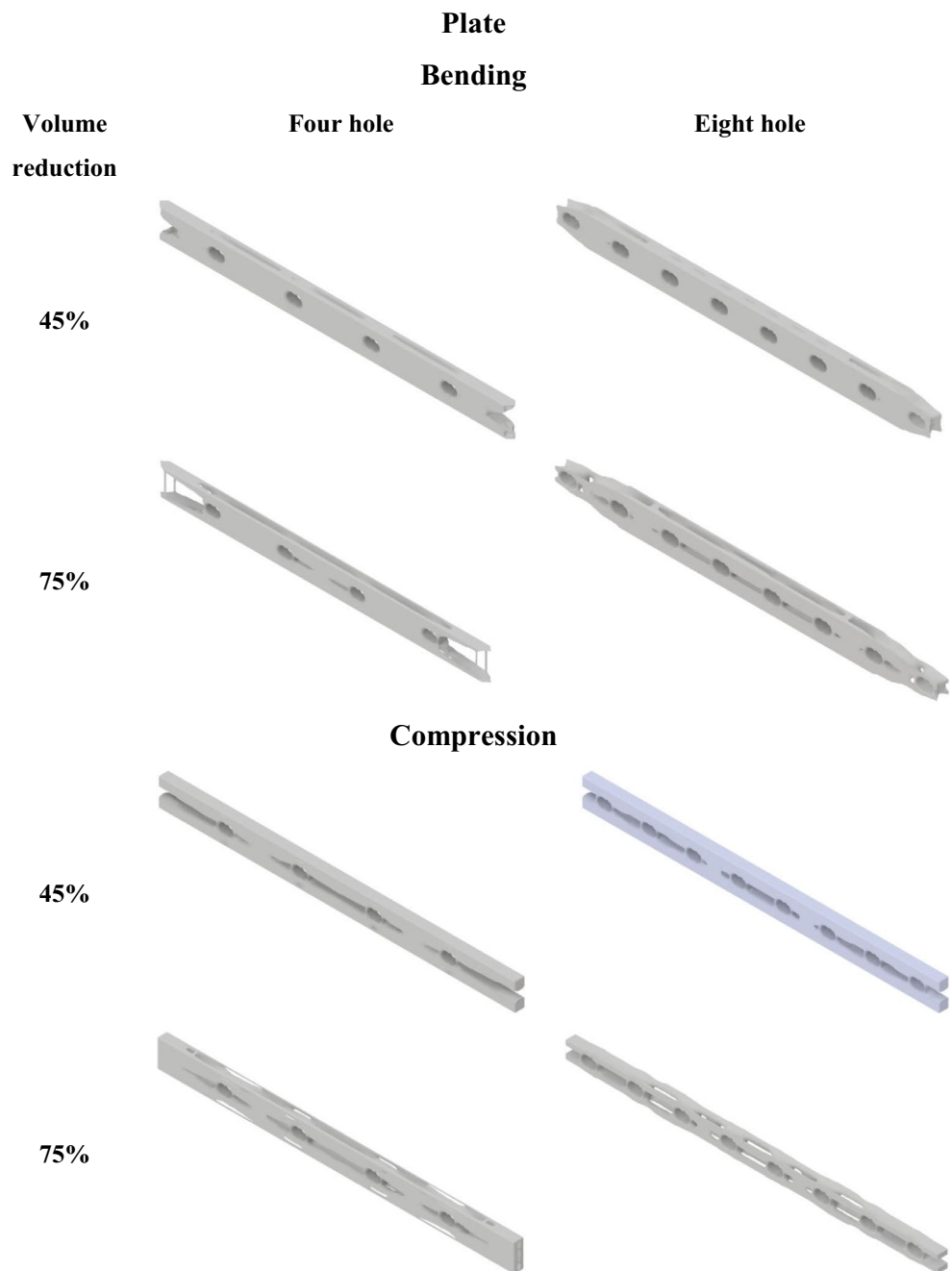


Fig. 4 Topology optimisation results of four-hole and eight-hole fracture plate considering bending and compression loads and 45% of volume reduction and 75% of volume reduction



10 Hz, and the mean slope of the curve (i.e. equivalent stiffness) was measured. The equivalent stiffness was obtained through the following procedure:

- i) From the tensile test and considering the linear elastic region, the following correlation, between applied force (F) and associated displacement (δ) determined by the extensometer, can be established as follows:

$$F = \kappa\delta \tag{4}$$

where κ is the equivalent stiffness.

- ii) Knowing the cross-section area and the initial length of each plate, Eq. (4) can be transformed into

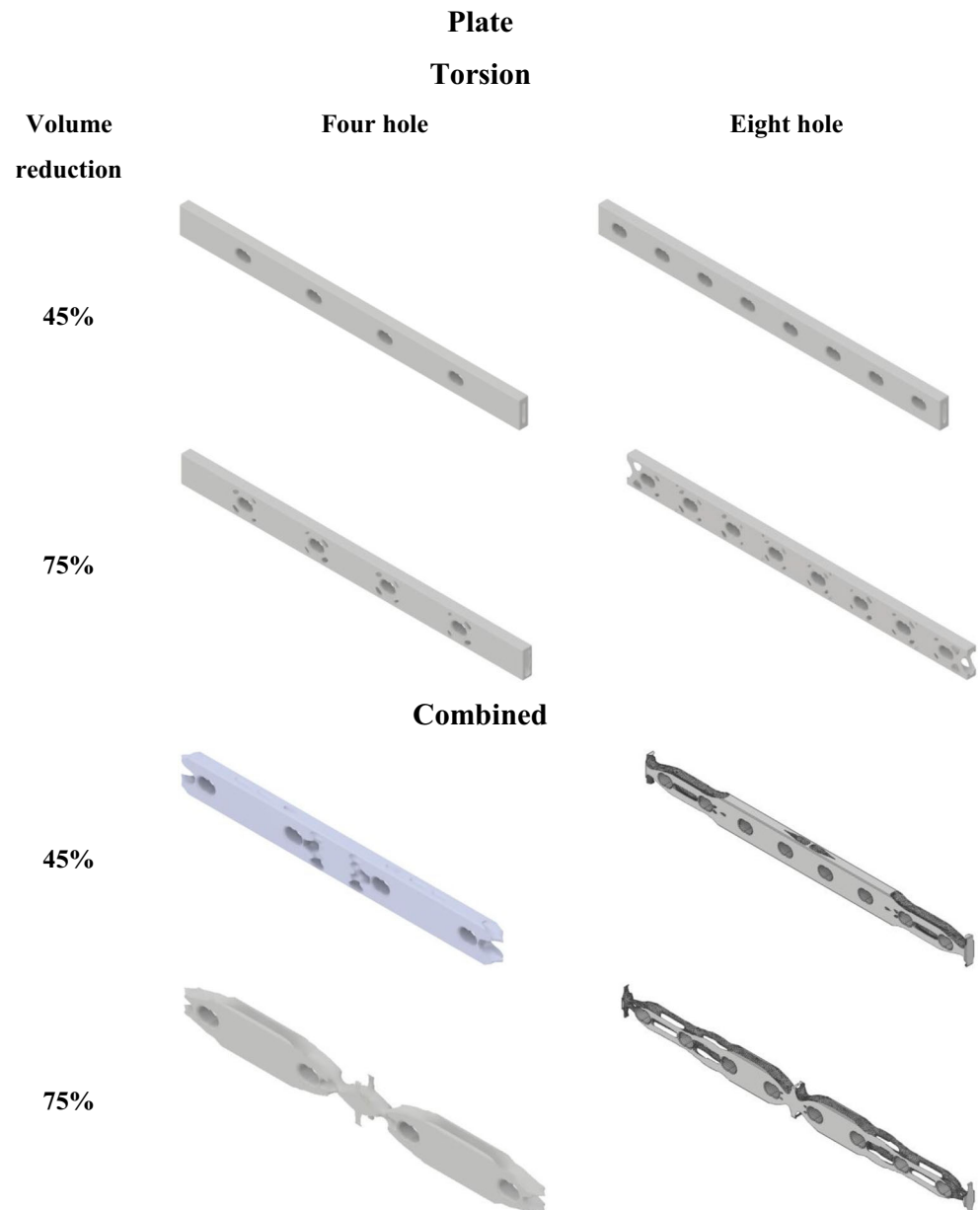
$$\sigma = E\varepsilon \tag{5}$$

where σ is the stress, ε is the strain and E is the equivalent elastic modulus determined from the slope of the stress strain curve.

4.5.2 Torsion test

Torsion tests were performed using a servo-hydraulic tension/torsion Instron® 8862 (Instron, USA) machine with a

Fig. 5 Topology optimisation results of four-hole and eight-hole fracture plate considering torsion and combined loads and 45% of volume reduction and 75% of volume reduction



maximum torque capacity of 1000 Nm and 45° deflection with a controlled deflection of 5°/min and an accuracy of $\pm 0.002\%$ of load cell capacity or 0.5% of indicated load. The strain was measured by a torsional Epsilon (Model 3350, Epsilon, USA) extensometer with a gauge length of 25 mm and a shear strain angle of $\pm 3^\circ$. Tests were performed in duplicate. Moment and deflection histories were documented, and the mean slope of the curve (i.e. equivalent stiffness in Nmm/rad) was measured.

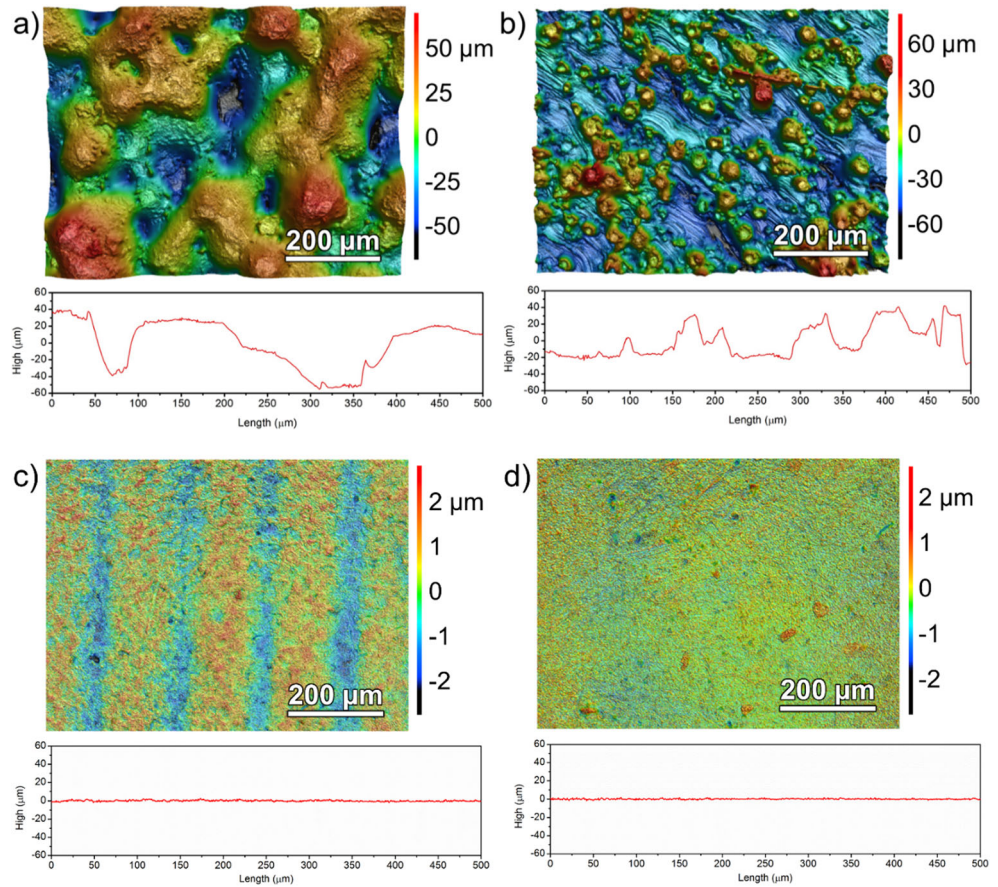
4.5.3 Four-point bending test

Four-point bending tests were performed following the British Standard (BSI) for determining the stiffness of a fixation plate

(BS 3531-23.1: 1991 ISO 9585:1990) using the Instron 5969 (Instron, USA) machine fitted with a 10 kN load cell with displacement rate of 1 mm/min and an accuracy of $\pm 0.4\%$ of reading down to 1/100 of load cell capacity. This test considers four rollers of 10 mm in diameter as shown in Fig. 2. The distance between the load and support rollers (h) and the load rollers span (k) values were 30.5 mm and 75 mm for the four-hole plate and 22.5 mm and 45 mm for the eight-hole plate. The displacement was measured using an Imetrum universal video extensometer (Flax Bourton, UK) with accuracy of $\pm 0.01\%$ strain, and three replicas were considered. The equivalent bending stiffness was measured as follows [11]:

$$S_B = \frac{(4h^2 + 12hk + k^2) \cdot Sh}{24} \quad (\text{N.m}^2) \quad (6)$$

Fig. 6 Surface map of $500 \times 750 \mu\text{m}^2$ and surface profile of $500 \mu\text{m}$ for **a** EBM and **b** SLM and **c** Biomet and **d** Synthes



where S_B is the bending stiffness and the slope (S) was measured from the load-displacement curve.

The equivalent bending elastic modulus was calculated as follows [12]:

$$E_B = 0.17L^3S/bd^3 \tag{7}$$

where E_B is the equivalent bending elastic modulus, L is the support span, b is the plate’s width, and d is the plate’s thickness.

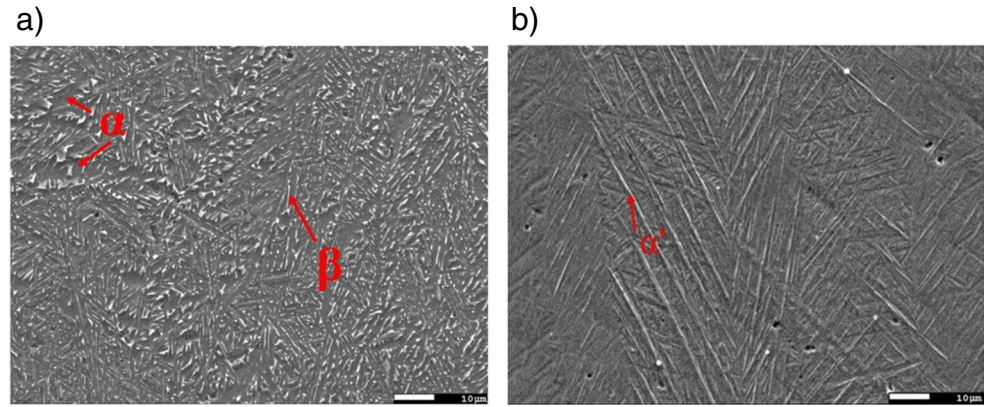
4.6 Tribological study

The wear performance of fixation plates is particularly important to minimise wear debris and ion release which can cause inflammation of surrounding tissues and potentially carcinogenic effects. Wear rate and coefficient of friction of both EBM and SLM plates were analysed using a pin-on-disc test (Pod-2, Teer Coatings Ltd., UK). An alumina bearing ball (Al_2O_3) with a 5-mm diameter was used as the friction pin (Ceratec Technical Ceramics, Netherlands). The pin-on-disc experiment was

Table 3 Characteristics of the EBM, SLM and commercial parts

Density (%)	EBM	SLM	Synthes	Biomet
	99.0 ± 0.01	98.0 ± 0.01	98.0 ± 0.01	96.0 ± 0.01
Surface roughness Ra (μm)	19.16 ± 4.94	15.11 ± 2.25	0.37 ± 0.04	0.45 ± 0.06
Overall composition (wt.%)				
Al	5.9	5.82	0	5.65
V	4.19	3.77	0	4.08
Ti	90.12	90.00	100	90.27
Hardness	337.40 ± 17.60	312.60 ± 7.37	268.20 ± 13.42	310.80 ± 7.79

Fig. 7 Microstructure of **a** EBM and **b** SLM



conducted for 9000 s, at a constant sliding speed of 5.24 cm/s and a constant load of 2, 6, 10 and 14 N. Tests were performed in triplicate, in a lubricated condition using phosphate-buffered saline (PBS) (Sigma-Aldrich, USA), under a controlled temperature of 37 °C. The coefficient of friction was recorded as function of time during the experiments.

The wear rates were calculated using the following equation [13]:

$$W = \frac{V}{F \cdot v \cdot t} \quad (8)$$

where W is the wear rate, F is the applied load, v is the sliding speed, and t is the duration of the experiment. The wear volumes (V) and wear tracks of the fixation plates after testing were estimated from surface scanners taken out by optical microscopy (VHX-500, Keyence, Japan). The wear tracks were also observed by scanning electron microscopy (Q-250, Thermo Fisher, Waltham, USA) in back-scattering

electron mode (BSE), and their chemical composition was analysed by energy dispersive X-ray spectroscopy (EDS), using an acceleration voltage of 20 kV.

4.7 Biological study

4.7.1 Cell culture/cell seeding

In vitro tests were performed using human adipose-derived bone osteosarcoma cells, Saos-2 (ATCC® HTB-85™) (ATCC, Manassas, VA, USA). Cells were cultured in T75 tissue culture flasks (Sigma-Aldrich, Dorset, UK) with McCoy's 5A Medium (ATCC® 30–2007™) (ATCC, Manassas, VA, USA) based media containing 15% foetal bovine serum, supplemented with penicillin and streptomycin (1%) until 80% confluence and harvest using 0.05% trypsin-EDTA solution (Thermo Fischer Scientific, Waltham, USA). After cell counting, cells were seeded on the fixation plates

Fig. 8 XRD of the EBM, SLM, Synthes and Biomet

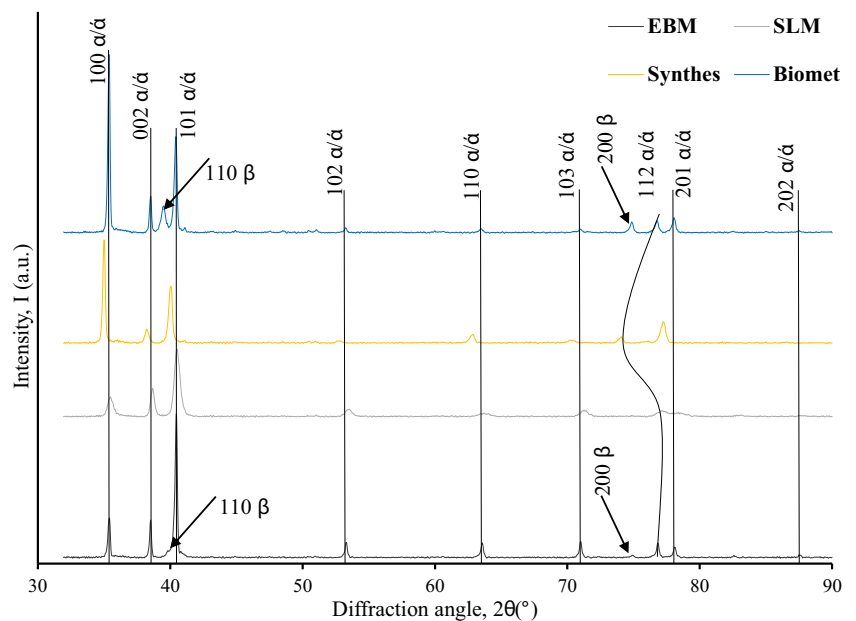
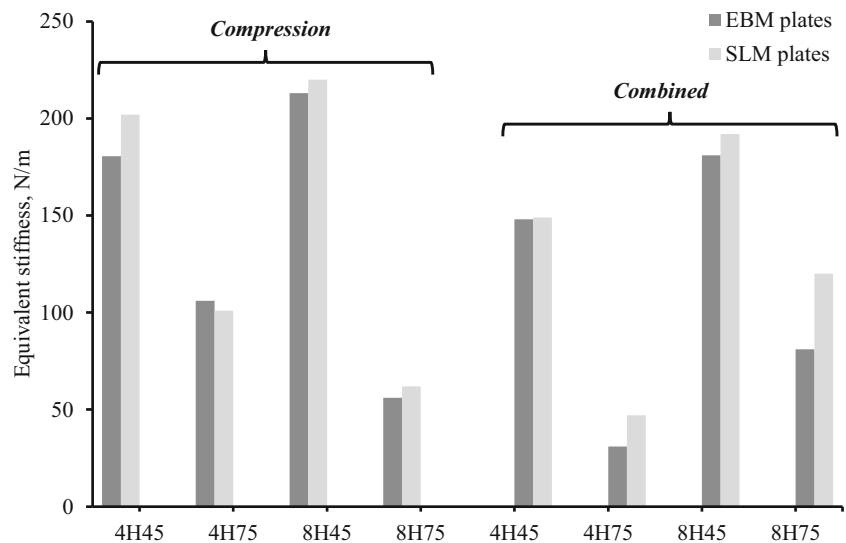


Fig. 9 Tensile equivalent stiffness of *compression* and *combined* optimised for both EBM and SLM plates. 4H45, four-hole plate with 45% volume reduction; 4H75, four-hole plate with 75% volume reduction; 8H45, eight-hole plate with 45% volume reduction; and 8H75, eight-hole plate with 75% volume reduction



(200 μL of media containing around 5×10^4 cells per sample) and incubated at standard conditions (37 $^\circ\text{C}$ under 5% CO_2 and 95% humidity) for 3 h to allow cell attachment, before the addition of 5 mL fresh based media.

4.7.2 Cell proliferation

Cell proliferation was assessed at 1, 4 and 7 days after cell seeding using the resazurin assay, also known as the Alamar Blue assay (reagents from Sigma-Aldrich, Dorset, UK). The media was changed every 3 days. At each time point, the cell-seeded plates were placed in a new 6-well plate, and 5 μL Alamar Blue solution 0.001% (v/v) in culture media was added to each well. The plates were incubated for 4 h under standard conditions. After incubation, 150 μL of each sample was transferred to a 96-well plate and the fluorescence intensity measured at 530 nm excitation wavelength and 590 nm

emission wavelength with a spectrophotometer (sunrise, Tecan Mannedorf, Zurich, Switzerland). Tests were performed in triplicate.

4.7.3 Cell viability

Laser confocal microscopy was employed to further examine cell viability through a Live/Dead stain kit (Thermo Fischer Scientific, Waltham, MA, USA) at day 4 and 7. The live/dead stain was prepared by adding 20 μL of 2 mM EtHD-1 stock solution to 10 mL of sterile phosphate bovine serum (PBS), and the reagents were combined via transferring 5 μL of 4 mM Calcein AM stock solution to the 10 mL EthD-1 solution. The resulted solution was then added directly to the plates. Confocal images were obtained using a Leica TCS SP5 (Leica, Milton Keynes, UK) confocal microscope.

Fig. 10 Equivalent torsional stiffness of the *torsion* optimised EBM and SLM plates. 4H45, four-hole plate with 45% volume reduction; 4H75, four-hole plate with 75% volume reduction; 8H45, eight-hole plate with 45% volume reduction; and 8H75, eight-hole plate with 75% volume reduction

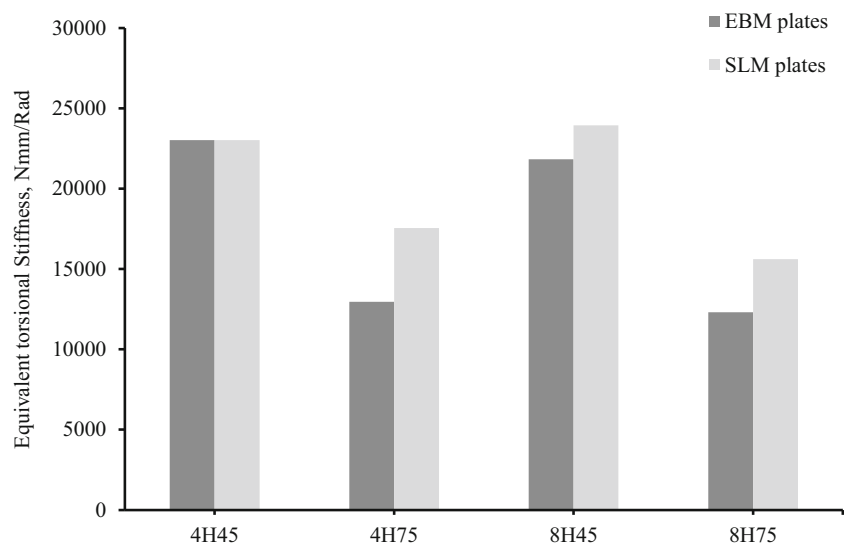
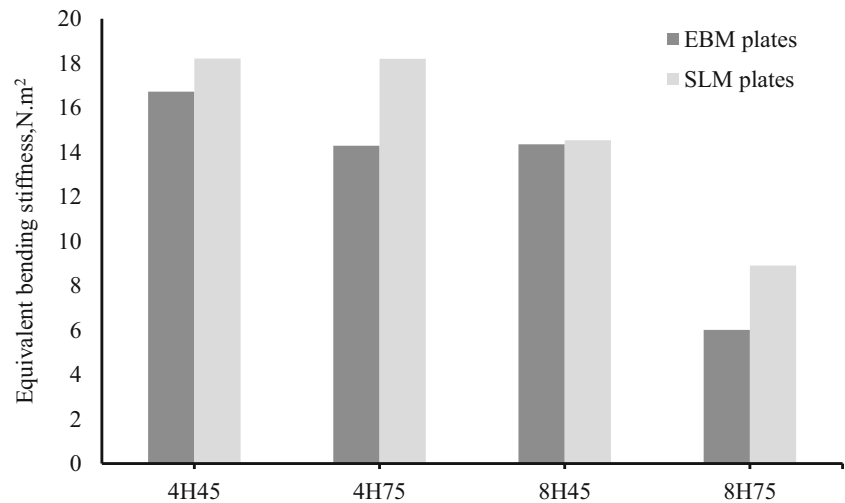


Fig. 11 Equivalent bending stiffness of initial and bending optimised cases of EBM and SLM plates considering a volume reduction. 4H45, four-hole plate with 45% volume reduction; 4H75, four-hole plate with 75% volume reduction; 8H45, eight-hole plate with 45% volume reduction; and 8H75, eight-hole plate with 75% volume reduction



4.8 Statistical analysis

Microhardness, surface roughness and tribological and biological results were analysed using Minitab 18 software (PA, USA). All studies were analysed using ANOVA to compare between the results. The data were also analysed using the Tukey post hoc test by specific pairwise comparisons. Significance was set at $p < 0.05$ with a confidence interval of 95%.

5 Results

5.1 Material composition, microhardness and surface roughness of printed fixation plates

The EBM and SLM fixation plates were vertically 3D printed to maximise the use of the working platform as shown in Fig. 3. Topology-optimised geometries are presented in Figs. 4 and 5. The surface map and surface profile of the

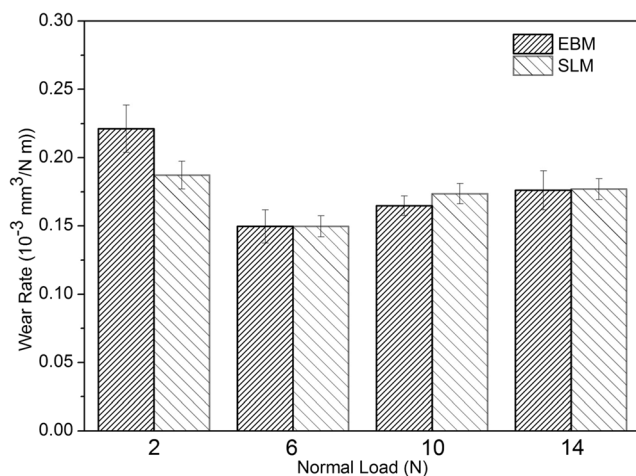


Fig. 12 Wear rate of EBM and SLM plates for different loads with corresponding standard deviations

fixation plates are presented in Fig. 6. The results of the surface roughness (Ra), density, chemical composition and microhardness of the EBM, SLM and commercial Synthes and Biomet fixation plates are shown in Table 3.

As observed EBM fixation plates present higher surface roughness compared to SLM and commercial Synthes and Biomet plates, statistical analysis shows that all plates were significantly different ($p < 0.05$). Results also seem to indicate high microhardness values for EBM fixation plates. However, in this case, no statistically significant differences ($p > 0.05$) were observed between the EBM, SLM and Biomet plates. The EDX results presented in Table 3 confirmed the initial powder composition provided by the suppliers. Results also show that commercial Synthes plates are 100% made of titanium, while the Biomet plates are made of Ti-6Al-4 V alloy with a composition similar to the printed plates.

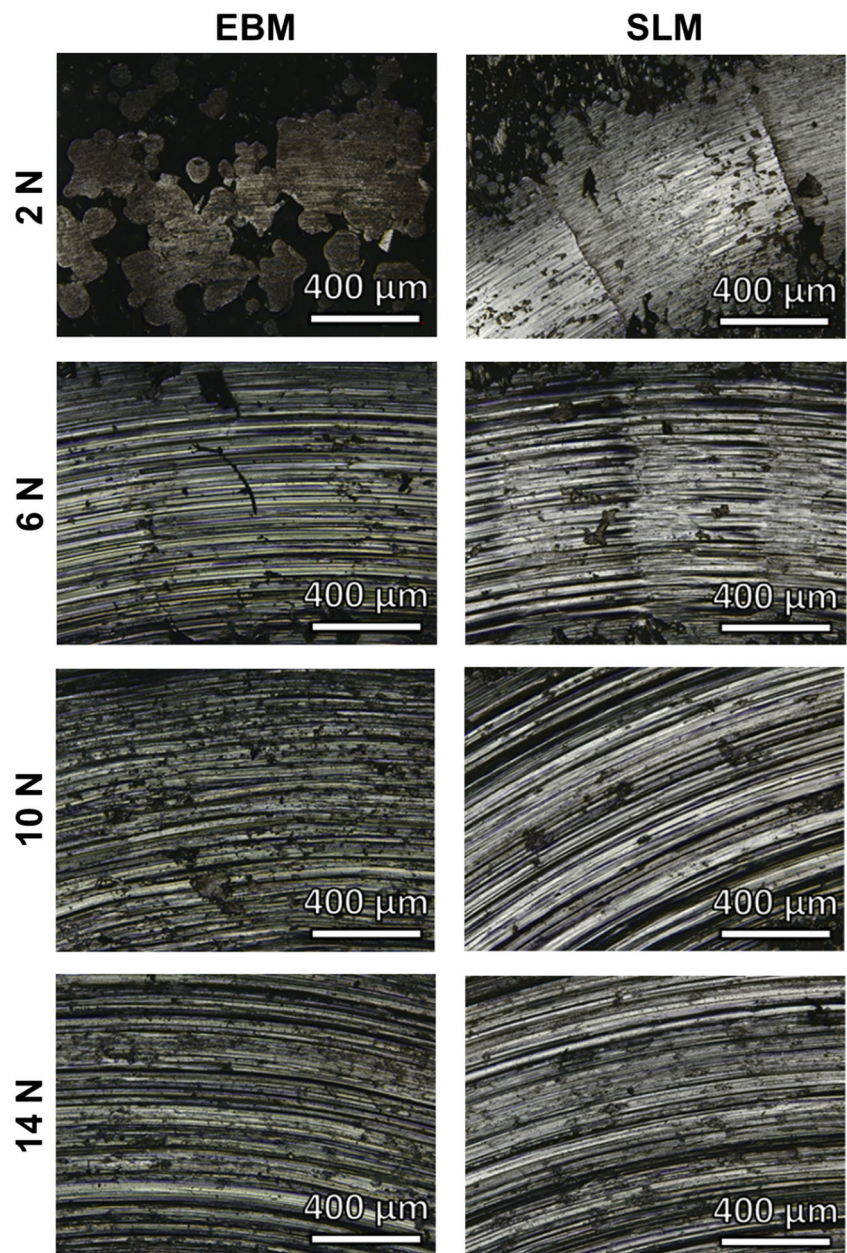
The microstructure of the EBM and SLM plates is shown in Fig. 7. The EBM plates consist of α and β alloys with the beta phase appearing at the grain boundaries. The SLM plates present martensitic α' needles. The XRD patterns of the fixation plates (Fig. 8) present similar diffraction patterns. However, it is possible to observe in the EBM and Biomet pattern, a peak of body-centred cubic β structure as pointed in Fig. 5a for EBM, while the other peaks are identified as α/α' , which cannot be differentiated as they show the same hexagonal close-packed structure. EBM plates show higher peak intensities than the SLM, which can be attributed to the rougher structure of the EBM fixation plates and a finer α' phase in the SLM fixation plates.

5.2 Mechanical performance of printed fixation plates

5.2.1 Tensile test

Tensile test results for both EBM and SLM plates are presented in Fig. 9. Results show that the equivalent

Fig. 13 Wear track of the EBM and SLM sample tested at 2, 6, 10 and 14 N obtained in the optical microscope



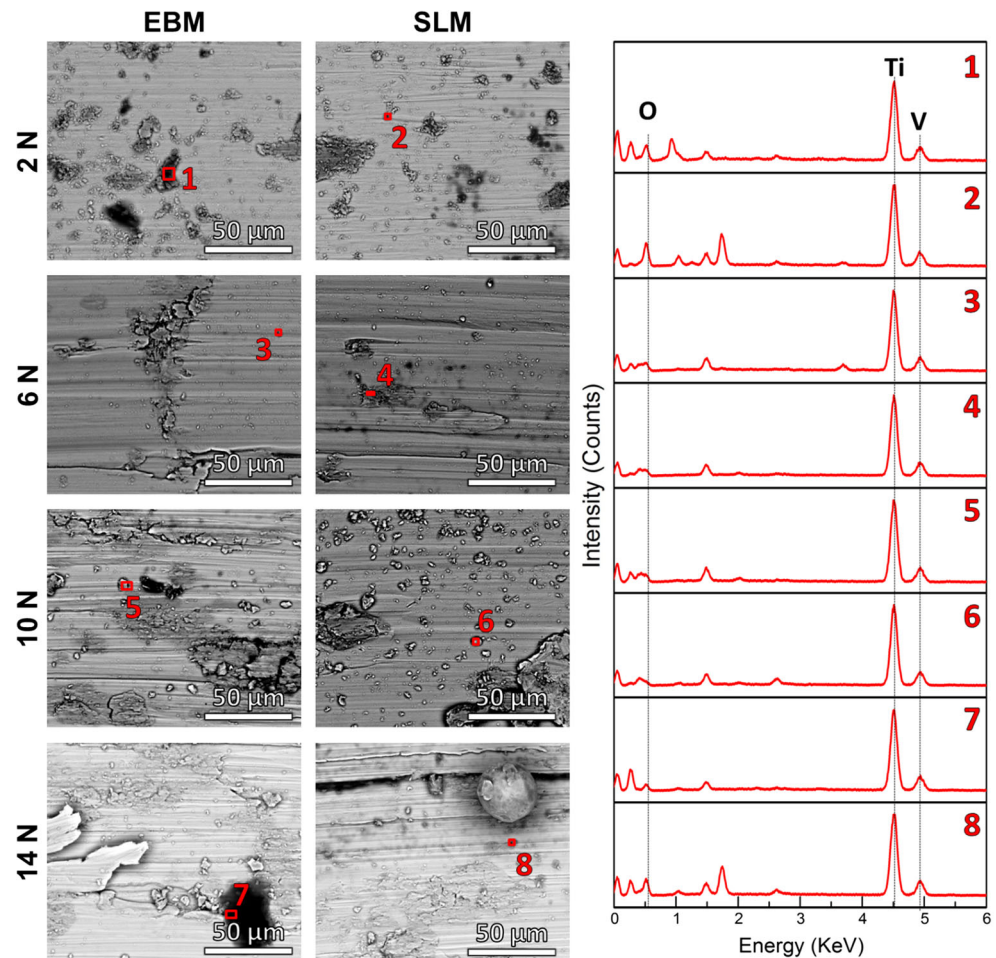
stiffness decreases by increasing the volume reduction. As observed for plates optimised for *compression* loads and 45% of volume reduction, SLM plates present higher equivalent stiffness than EBM plates. Differences between SLM and EBM plates seem to decrease by increasing the number of holes. In the case of plates containing eight holes and optimised for 75% of volume reduction, the SLM plates present slightly high equivalent stiffness. For the four-hole plates optimised for 75% of volume reduction, EBM plates present slightly high equivalent stiffness. In the case of plates optimised for *combined* loads, SLM plates present higher equivalent stiffness than EBM plates, except for four-hole plates and 45% of

volume reduction in which the equivalent stiffness of both EBM and SLM plates is similar.

5.2.2 Torsion test

The equivalent torsional stiffness results are presented in Fig. 10. Results show that the equivalent torsional stiffness decreases by increasing volume reduction. SLM plates present high equivalent torsional stiffness, except for four-hole plates and 45% of volume reduction in which the equivalent torsional stiffness of both EBM and SLM plates is similar. The equivalent torsional stiffness differences between EBM and SLM plates seem to increase by increasing the volume reduction.

Fig. 14 BSE images of the wear track of the EBM and SLM plates tested at 2, 6, 10 and 14 N at $\times 1000$ magnifications with the EDS spectrums



5.2.3 Bending test

The resulted equivalent bending stiffness for both EBM and SLM fixation plates is shown in Fig. 11. The equivalent bending stiffness decreases by increasing the volume reduction. In all cases, SLM fixation plates present high equivalent bending stiffness. Results also show that by increasing the volume reduction, the equivalent bending stiffness differences between EBM and SLM plates increases.

5.3 Tribological study

The wear rate values of both the EBM and SLM plates are presented in Fig. 12. High wear rates ($0.22 \pm 0.02 \times 10^{-3} \text{ mm}^3/\text{Nm}$ for EBM plates and $0.19 \pm 0.01 \times 10^{-3} \text{ mm}^3/\text{Nm}$ for SLM plates) are observed for the 2 N load. For 6 N, the wear rate values decrease ($0.15 \pm 0.01 \times 10^{-3} \text{ mm}^3/\text{Nm}$ for both plates) and increase again by increasing the load. At 14 N, the wear rate values are $0.18 \pm 0.01 \times 10^{-3} \text{ mm}^3/\text{Nm}$ for EBM plates and $0.17 \pm 0.01 \times 10^{-3} \text{ mm}^3/\text{Nm}$ for SLM plates. Figure 13 shows a view map of the wear tracks obtained by optical microscopy.

The wear stages comprise delamination, ploughing, grooving and oxidation. The delamination is shown as the perpendicular lines of the wear direction. These lines are larger for lower loads and decrease in size with the increase of the load value. The wear tracks of both EBM and SLM plates tested under the same load present similar profiles and track width. At low load values, high penetration depths are observed in the EBM plates. At the highest load, 14 N, the EBM fixation plates present a lower depth of penetration of $125 \pm 5 \mu\text{m}$, and for the SLM, the depth of penetration is $136 \pm 4 \mu\text{m}$. From the wear tracks, it is possible to observe that the worn surfaces of loads higher than 2 N displayed plastic deformation (ploughing) highlighted by the presence of grooves. These grooves on the plates shown as lines marked parallel to the sliding direction are a result of the hard alumina ball being in contact against the plates. The grooves increase and became more visible when the load increases. The EDS spectrums for the EBM and SLM plates at all considered loads are presented in Fig. 14. An oxide debris was found on both plates between an atomic weight of 40–70%. Plates conveyed small traces of Na and Cl due to the PBS solvent.

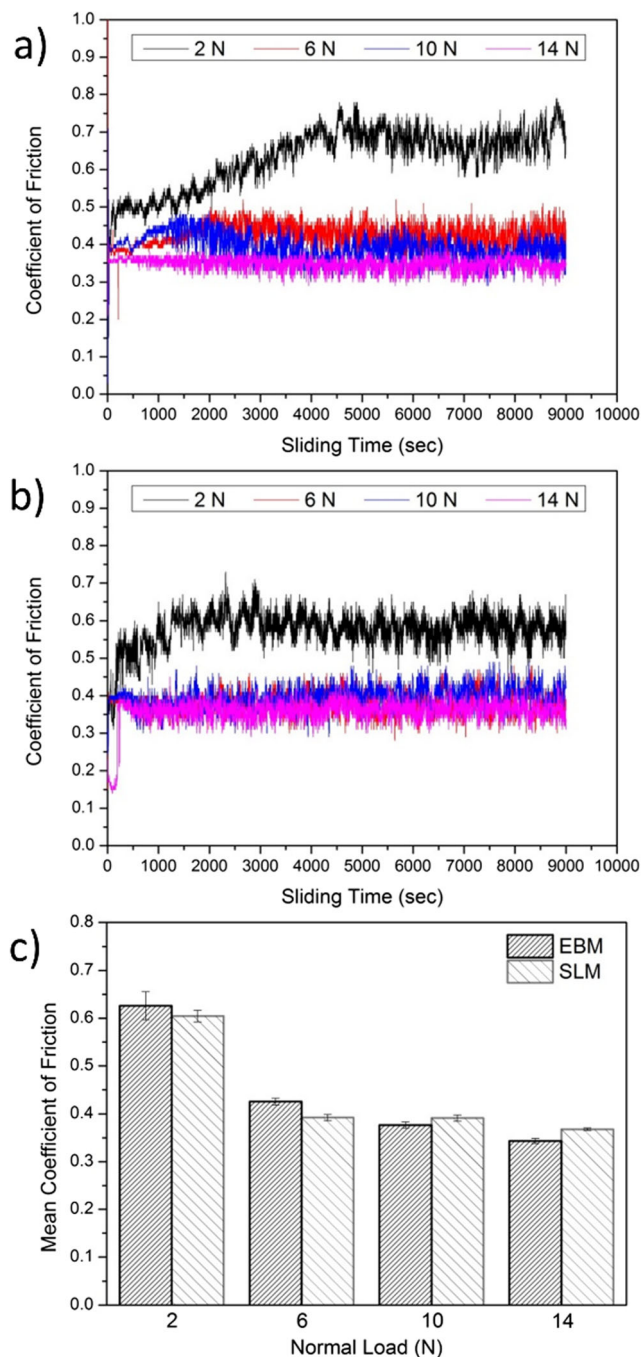


Fig. 15 Evolution of the coefficient of friction with the time for the **a** EBM and **b** SLM and **c** mean of coefficient of friction at the steady state of EBM and SLM plates with corresponding standard deviations

The variation of the coefficient of friction considering different loading values (2, 6, 10 and 14 N) applied for 9000 s are shown in Fig. 15 a and b. Four stages are observed. First, the coefficient of friction exhibits an initial increment until a local maximum, due to the contact between the ball and the plates surface. Then, the coefficient of friction decreases reaching a minimum due to the formation of an oxide layer [14]. In the third stage, the coefficient of friction increases resulting from the elimination of the oxide layer due to the erosion and the

stresses caused by the surface plastic deformation produced during the wear tests [14]. Finally, the coefficient of friction reaches a steady state after ~4000 s. The SLM fixation plates present lower oscillations and better stability of coefficient of friction than EBM plates. However, there are no significant differences ($p > 0.05$) between the EBM and SLM steady state coefficient of friction.

5.4 Biological properties

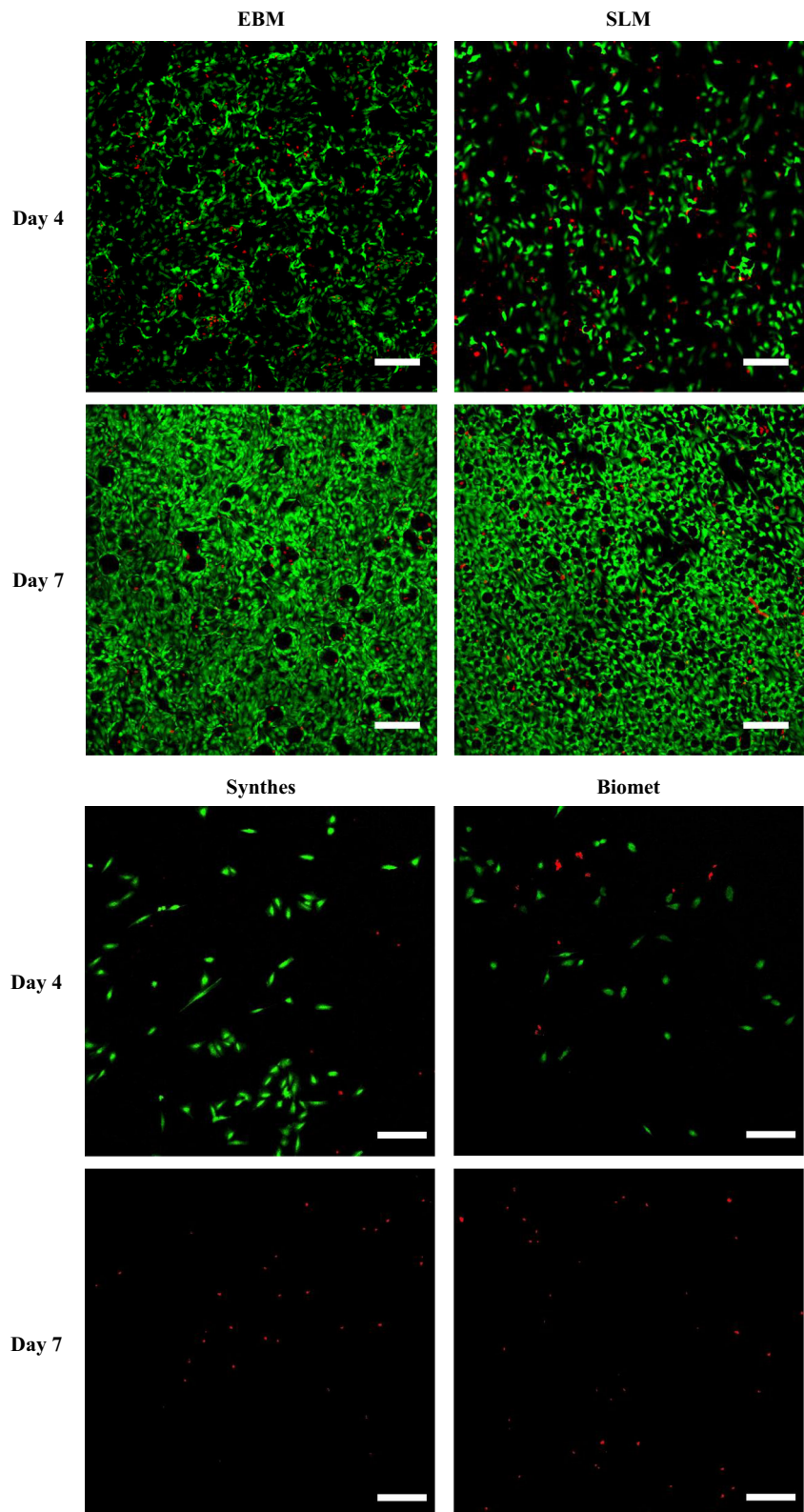
Figure 16 presents the live/dead assay results showing live (green) and dead (red) cells on the fixation plates after 4 and 7 days of cell seeding. Results show that cells were not able to attach and proliferate on the commercial plates, while in the case of both EBM and SLM fixation plates, cells are proliferating creating cell-cell network with very few cells dying. These results are confirmed by the Alamar Blue assay (Fig. 17) showing an increase in fluorescence intensity (measuring the metabolic activity of cells) with time in the case of EBM and SLM plates. At day 7, higher fluorescence intensity values are observed for the EBM plates in comparison to the SLM ones. This can be explained by the high surface roughness of the EBM plates that promotes cell attachment and proliferation, yet not high enough to compromise cell-cell networks interaction. High metabolic cell activity (fluorescence intensity) is also observed in EBM and SLM fixation plates in comparison to commercial ones.

6 Discussion

As a consequence of the fabrication procedure, 3D printed plates present higher surface roughness than commercial plates. The surface roughness depends on the raw powder properties (e.g. particle size) and processing conditions (e.g. scan speed and layer thickness). Results show that EBM fixation plates present higher surface roughness than SLM fixation plates. This is due to the large powder particle size (45 to 100 μm for EBM and 25 to 45 μm for SLM), high scan speed (4530 mm/s for EBM and 375 mm/s for SLM) and high layer thickness (50 μm for EBM and 30 μm for SLM).

A similar raw powder composition was used for both EBM and SLM process. However, EBM and SLM fixation plates present a different microscopic structure due to the different heating and cooling cycles. In the case of EBM plates, printed under vacuum, the slow cooling rates due to the high temperature of the substrate is responsible for the presence of the α' phase instead of the α' . In the case of SLM plates, printed in an inert environment using Argon, the low temperature of the substrate plate causes a faster solidification leading to the α' martensitic transformation. In the case of SLM plates, the fast cooling rates also induces a superior growth orientation of the α' plates as observed from Fig. 5b, showing the martensitic

Fig. 16 Live and dead assays of EBM, SLM, Synthes and Biomet plates on day 4 and day 7. Scale bar is 200 μm



needles mostly inclined towards the build direction at $\sim 40^\circ$. Results presented in Table 3 show that EBM fixation plates present slightly high microhardness than SLM fixation plates. This can be explained by the grain boundary and size (Fig. 5a)

and the fact that the EBM α needles are smaller and more compact than the ones observed in the SLM fixation plates.

The tensile, torsion and bending tests show that the SLM fixation plates present higher equivalent stiffness than the

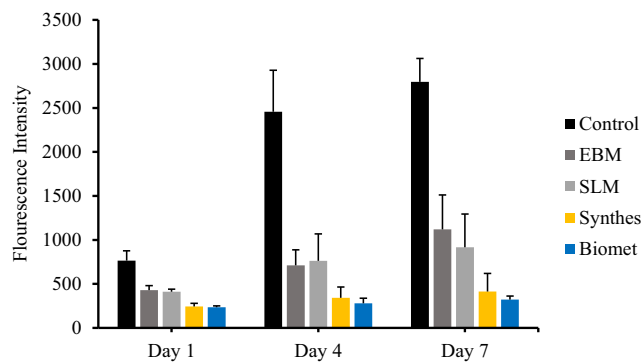


Fig. 17 Fluorescence intensity values of the fixation plates versus the control with corresponding standard deviations

EBM plates. This can be explained by the α' presence in the microstructure of the SLM plates and the α lamellar structure of the EBM [8]. Mechanical tests also show that topology-optimised plates present reduced equivalent stiffness for high volume reductions. As observed, the mechanical performance of the optimised plates tends to approach the mechanical properties of natural bone. This was observed in the case of the fixation plate optimised using *compression* load with 75% of volume reduction and eight-screw holes, where 3D printed plates using both EBM and SLM present an equivalent elastic modulus of 20 and 22 GPa respectively, in the range of natural cortical bone (15–25 GPa) [3, 4]. Other designs also tend to the cortical bone region such as the eight-hole plate optimised for *combined* loads with 75% of volume reduction 3D printed by EBM. However, the equivalent bending modulus of the *bending* optimised plates (28 GPa for the eight-hole with 75% of volume reduction) is slightly higher than the bending modulus of the natural cortical bone (9.82–15.7 GPa) [4, 15].

Wear results show that the highest wear rates occur for the lowest load (2 N), due to the rubbing of the counter part on the sample surface, resulting in insignificant plastic deformation. As reported by Hiksakado [16], for low loads, the wear rate is mainly affected by the surface roughness with the hardness and microstructure not playing a significant role. This explains the higher wear rate observed for the EBM and the high coefficient of friction at 2 N. However, Hatchings [17] shows that for higher loads, the surface hardness plays a major role on the wear resistance. This can explain the similar wear rate values of both EBM and SLM plates for higher loads (6 N, 10 N and 14 N). For high load regimes, the wear rate increases by increasing the load as more volume is removed from the plate. All printed plates present acceptable wear resistance values [14].

As reported by Sing et al. [18], cell to cell network is significantly affected by the surface characteristics such as the surface roughness. In this paper, the EBM and SLM plates were not post-processed in order to investigate if further post-processing is necessary to acquire adequate cell attachment and proliferation. This is to circumvent costly procedures such

as surface finishing and polishing. Results show that EBM plates present higher surface roughness than SLM fixation plates. Previously, Ponader et al. [20] reported that EBM parts with Ra higher than 56.9 μm presented limited cell-cell interactions, parts with Ra lower than 24.9 μm presented higher cell proliferation and attachment, and that the best results in terms of both cell attachment and proliferation were obtained for smooth surface parts (Ra of 0.07 μm). However, our results show high cell viability and proliferation results in EBM parts with surface roughness Ra of $19.16 \pm 4.94 \mu\text{m}$ indicating that no surface post-processing (e.g. grinding and polishing) is required. Cell proliferation studies using osteosarcoma cells show that, contrary to commercial plates, both EBM and SLM plates are able to sustain cell attachment and proliferation. These results show that the surface roughness of printed plates is acceptable not compromising the establishment of cell-cell interaction. Live/dead results also show that due to limited cell attachment to commercial plates, cells tend to die.

7 Conclusion

This paper shows that the combined use of topology optimisation with powder bed fusion is a viable approach to produce metallic fixation plates with improved mechanical performance (i.e. reduced equivalent stiffness and consequently bone loss problems). This approach allows to obtain lightweight fixation plates (a maximum of 75% of volume reduction was successfully considered) also reducing the cost of the plates. SLM plates present higher mechanical properties than EBM plates, while EBM plates present higher wear resistance, microhardness and surface roughness compared to SLM plates. Biological results also confirm that the obtained surface roughness values of both EBM and SLM plates are acceptable with 3D printed plates showing a significantly better capability to support cell attachment and proliferation.

Acknowledgements Authors are grateful for the support provided by the Saudi Arabian government and the South Manchester Hospital, Royal College of Surgeons. The first author is also grateful for the support of the Advanced Manufacturing Institute (AMI), King Saud University, Riyadh, Saudi Arabia. Mechanical tests were conducted with the support of Mr. Chris Cowan in the National Composites Certification and Evaluation Facility (NCCF), University of Manchester, Manchester, UK.

Open Access This article is licensed under a Creative Commons Attribution 4.0 International License, which permits use, sharing, adaptation, distribution and reproduction in any medium or format, as long as you give appropriate credit to the original author(s) and the source, provide a link to the Creative Commons licence, and indicate if changes were made. The images or other third party material in this article are included in the article's Creative Commons licence, unless indicated otherwise in a credit line to the material. If material is not included in the article's Creative Commons licence and your intended use is not permitted by statutory regulation or exceeds the permitted use, you will need to obtain

permission directly from the copyright holder. To view a copy of this licence, visit <http://creativecommons.org/licenses/by/4.0/>.

References

1. Johnell O (1997) The socioeconomic burden of fractures: today and in the 21st century. *Amer J Med* 103:S20–S26. [https://doi.org/10.1016/s0002-9343\(97\)90023-1](https://doi.org/10.1016/s0002-9343(97)90023-1)
2. Green M, Wishart N, Young E (2017) NJR 14th Annual Report. *Natl Jt Regist Annu Rep*. <http://www.njrreports.org.uk/Portals/0/PDFdownloads/NJR%2014th%20Annual%20Report%202017.pdf>
3. Jo M, Tencer A, Gardner M (2014) Biomechanics of fractures and fracture fixation. In: Court-Brown C, Heckman J, McQueen M, Ricci W, Tornetta P III, McKee M (eds) *Rockwood and Green's Fractures in Adults*. Lippincott Williams & Wilkins
4. McNamara L (2017) Bone as a material. In: Ducheyne P (ed) *Comprehensive Biomaterials II*. Elsevier, pp 202–227
5. Al-Tamimi A, Fernandes P, Peach C, Cooper G, Diver C, Bartolo P (2017) Metallic bone fixation implants: a novel design approach for reducing the stress shielding phenomenon. *Virtual Phys Prototyp* 12:141–151. <https://doi.org/10.1080/17452759.2017.1307769>
6. Bendsøe M, Sigmund O (2004) *Topology optimization: theory, methods, and applications*. Springer, Berlin
7. Murr L (2015) Metallurgy of additive manufacturing: examples from electron beam melting. *Addit Manuf* 5:40–53. [j.addma.2014.12.002](https://doi.org/10.1016/j.addma.2014.12.002)
8. Khorasani A, Gibson I, Awan U, Ghaderi A (2019) The effect of SLM process parameters on density, hardness, tensile strength and surface quality of Ti-6Al-4V. *Addit Manuf* 25:176–186. <https://doi.org/10.1016/j.addma.2018.09.002>
9. Al-Tamimi A, Huang B, Vyas C, Hernandez M, Peach C, Bartolo P (2019) Topology optimised metallic bone plates produced by electron beam melting: a mechanical and biological study. *Int J Adv Manuf Tech*. <https://doi.org/10.1007/s00170-019-03866-0>
10. Denry I, Holloway J (2004) Elastic constants, Vickers hardness, and fracture toughness of fluorrichterite-based glass–ceramics. *Dent Mater* 20:213–219. [https://doi.org/10.1016/s0109-5641\(03\)00094-0](https://doi.org/10.1016/s0109-5641(03)00094-0)
11. British Standard (1991) *Implants for osteosynthesis – Part 23: bone plates – Section 23.1 Method for determination of bending strength and stiffness, BS 3531–23.1:1991 ISO 9585:1990*, British Standard
12. Standard ASTM (2017) *Standard test method for flexural properties of unreinforced and reinforced plastics and electrical insulating materials by four-point bending, D6272–17*. Standard, ASTM
13. Zmitrowicz A (2006) Wear patterns and laws of wear – a review. *J Theoretical Appl Mech* 44:219–253
14. Toh W, Wang P, Tan X, Nai M, Liu E, Tor S (2016) Microstructure and wear properties of electron beam melted Ti-6Al-4V parts: a comparison study against as-cast form. *Metals*. 6:284. <https://doi.org/10.3390/met6110284>
15. Keller T, Mao Z, Spengler D (1990) Young's modulus, bending strength, and tissue physical properties of human compact bone. *J Orthop Res* 8:592–603. <https://doi.org/10.1002/jor.1100080416>
16. Hisakado T (1977) The influence of surface roughness on abrasive wear. *Wear*. 41:179–190. [https://doi.org/10.1016/0043-1648\(77\)90200-9](https://doi.org/10.1016/0043-1648(77)90200-9)
17. Hutchings I (1992) *Tribology: friction and wear of engineering materials*, 1st edn. Butterworth-Heinemann
18. Sing S, An J, Yeong W, Wiria F (2016) Laser and electron-beam powder-bed additive manufacturing of metallic implants: a review on processes, materials and designs. *J Orthop Res* 34:369–385. <https://doi.org/10.1002/jor.23075>

Publisher's note Springer Nature remains neutral with regard to jurisdictional claims in published maps and institutional affiliations.